Geophys. J. Int. (2002) **151,** 416–426

Three-dimensional calculations of fault-zone-guided waves in various irregular structures

Gunnar Jahnke,[1] Heiner Igel[1] and Yehuda Ben-Zion[2]

[1] *Department für Geound Umweltwissenschaften, Ludwig-Maximilians-Universität, München, Germany. E-mail: igel@geophysik.uni-muenchen.de*
[2] *Department of Earth Sciences, University of Southern California, Los Angeles, USA*

Accepted 2002 May 13. Received 2002 April 6; in original form 2001 October 16

SUMMARY

The detailed structure of fault zones (FZs) plays an important role in problems related to fault mechanics, earthquake rupture, wave propagation and seismic hazard. FZs are thought to consist of an O(10–100) m wide region of decreased seismic velocity but structural details such as their depth extent, lateral and vertical variations, etc. are elusive. The small spatial scales involved make such structures difficult to image with ray-theoretical methods such as tomography. However, seismic energy trapped inside FZ layers can provide dispersive wave trains that carry information on the FZ structure. These waves can travel many kilometres inside the FZ before reaching the surface and are therefore strongly altered by its properties. Candidate trapped waves have been observed above several active faults. Inversion algorithms exist that can model these observations in terms of planar fault zone structures. However, at present it is not clear how reliable these estimates are, as the effects of (even small) 3-D variations on trapped waves are not well understood. The goal of this study is to distinguish 3-D structures that do and do not significantly affect FZ waves. To achieve this, we perform numerical calculations of wave propagation in various FZ geometries and analyse the waveforms, spectra and envelopes of the synthetic seismograms. The main results are that (1) moderate changes of the shape of FZ or (2) small-scale heterogeneities or (3) depth-dependent properties do not strongly affect the observed FZ waves. In contrast, strong effects are to be expected from (4) breaks in the continuity of FZ structure (e.g. offsets), which may at some point allow imaging of such features at depth.

Key words: 3-D effects, fault zones, finite differences, guided waves.

1 INTRODUCTION

Recently, data with evidence of fault-zone- (FZ-) guided head and trapped waves have been recorded in the vicinity of several earthquake faults. FZ head waves propagate along material interfaces in the FZ structure, while trapped waves propagate within low-velocity FZ layers. Detailed descriptions of theoretical properties of these waves in ideal 2-D homogeneous seismic waveguides can be found in Ben-Zion & Aki (1990) and Ben-Zion (1998). Early observations of FZ-guided waves were reported by Fukao *et al.* (1983), Leary *et al.* (1987), Li & Leary (1990), Ben-Zion & Malin (1991) and Ben-Zion *et al.* (1992). Li *et al.* (1994, 1998) and Peng *et al.* (2000) analysed candidate trapped waves generated by aftershocks along segments of the rupture zone of the 1992 M7.3 Landers, California, earthquake. Hough *et al.* (1994) obtained images of several small fault segments in the aftershock area of the 1992 M6.1 Joshua Tree earthquake based on modelling of candidate head waves. A summary of additional observations of FZ-guided waves can be found in Ben-Zion & Sammis (2002). The results from these studies suggest that FZ structures at depth may have coherent layers of damaged rock, with low seismic velocity and high attenuation, that are tens to hundreds of metres wide. The boundary of the FZ layers may be abrupt or gradual with a smooth transition zone characterized by intermediate seismic properties.

To understand the properties of seismic FZ waves and the conceptual issues of the representation theorem associated with sources at material interfaces, 2-D analytical solutions for plane-layered structures were developed (Ben-Zion 1989, 1990, 1999; Ben-Zion & Aki 1990). These solutions are now employed efficiently as kernels in inversions of observed data using grid search and genetic algorithm techniques (Michael & Ben-Zion 1998; Ben-Zion *et al.* 2002). However, the 2-D analytical solutions cannot be used to study properties of guided waves in general 3-D structure. Calculations of wave propagation through irregular structures were performed using ray-theoretical techniques (Cormier & Spudich 1984; Cormier & Beroza 1987) and numerical methods (Leary *et al.* 1991, 1993; Igel *et al.* 1991, 1997; Li *et al.* 1994; Huang *et al.* 1995; Li & Vidale 1996). Most of these investigations were carried out using either 2-D or acoustic approximations. A systematic examination of deviations from planar FZ structure, complete

3-D elastic effects, and a discussion on the implications for inverse imaging schemes (e.g. Michael & Ben-Zion 1998) is still missing. The present paper aims at filling this gap by performing a parameter space study with various likely 3-D FZ structures. In a companion paper (Igel *et al.* 2002), the numerical method used in this study (high-order finite-difference method) is introduced and comparisons of analytical and numerical solutions for strike-slip sources at material interfaces are presented. Igel *et al.* (2002) also provide some examples of 3-D wave effects associated with heterogeneous FZ structures. The main goals of our 3-D parameter space study are to clarify (1) under what conditions the imaging of FZ structures can be done using analytical methods for planar FZ structures and (2) which deviations from simple FZ structures may be detectable with 3-D methods. The focus is on FZ trapped waves. Prominent generation of FZ head waves requires an overall property contrast across the fault, which is not considered in detail here. The results indicate that structural discontinuities larger than the FZ width and source distance from the fault are significant perturbations that can destroy the generation and propagation efficiency of guided waves. On the other hand, the vertical gradient of properties and heterogeneity with a correlation length smaller than the FZ width do not inhibit guided wave propagation, nor can they be constrained by observations of guided waves. Various other cases fall on intermediate ground and have modest effects on the FZ waves.

2 NUMERICAL METHOD

To solve the 3-D elastic wave equation we use a fourth-order staggered-grid finite-difference (FD) method with an operator length of four grid points (Virieux 1984, 1986). The models used in this study are defined on a 3-D Cartesian staggered grid with an overall mesh size on the order of 200^3 grid points. We verified that the source, receivers and discontinuities in our models were implemented correctly, and that the method was able to produce accurate seismograms for 3-D geometries even with abrupt changes of the seismic properties, by comparison with existing analytic solutions (Ben-Zion 1990, 1999) in a previous paper (Igel *et al.* 2002). The grid spacing of our models is between 10 and 30 m and the corresponding minimum wavelengths considered in our simulations are ≈200–600 m. The source used in this study is a double couple with non-zero moment tensor components $M_{xy} = M_{yx} = M_0$. It is equivalent to a horizontal slip on a vertical plane, which is strike-slip faulting, a common source mechanism in transform fault zones. The source time function is the first derivative of a Gaussian function with a mean frequency ranging from 4.5 to 13.5 Hz.

3 RESULTS OF FAULT ZONE SIMULATIONS

In the following we investigate the effects of fault zones with 3-D geometry and property distribution on the generation of fault-zone-guided waves. The sequence of 3-D models has been chosen in order to develop incrementally intuition for the 3-D effects. We begin by introducing (1) a basic 2-D FZ structure as a reference solution. Then we investigate: (2) the effects of source location with respect to the FZ; (3) discontinuous FZ structures; (4) moderate changes to the shape of the FZ boundaries (narrowing and widening); (5) small-scale heterogeneities inside the FZ; (6) low-velocity surface layer at the top and depth-dependent velocities; and finally (7) FZ structures discontinuous at the surface but connected at depth. Unless otherwise mentioned, all models have the properties listed in Table 1. The seismogram plots show the *y*-component of velocity that—for the source–receiver geometry and the source mechanism chosen—represents predominantly *SH*-type motion.

3.1 Source location

The first model examines the sensitivity of the wavefield to the hypocentre location with respect to a basic 2-D coherent FZ structure. This model type can be calculated analytically. However, as we refer to these models when discussing 3-D perturbations, it is an important starting point. The model consists of a homogeneous FZ layer in a half-space. For a complete description of the model geometry see Fig. 1 and Table 1. For this setup, the trapped wave energy is greatest when the source is located directly at the FZ boundary (Fig. 2). The maximum amplitude of the trapped waves is 10 times larger than the maximum direct *S*-wave amplitude. For a source centred in the FZ, weaker trapped waves occur because of destructive interference for reasons of symmetry. The source located one FZ width outside the structure leads to an amplitude distribution along the receiver line, which is similar to the amplitude distribution of the direct *S* wave. In this case the amplitudes of the FZ waves are at most twice the *S*-wave amplitude. Strong effects can also be seen in the waveforms, amplitude spectra and the envelopes of the traces (Fig. 3): for the source at the FZ boundary the FZ wave energy is

Table 1. General properties of the simulations done in this study. The host rock of all models except the gradient model has identical seismic properties. The contrast of the model with small-scale inhomogeneities varies from 0 to 30 per cent. The contrast of all remaining models is 30 per cent.

	v_p (km s^{-1})	v_s (km s^{-1})	ρ (g cm^{-3})
Host rock	5.00	3.10	2.35
FZ			
Gradient model (at surface)	3.50	2.17	1.64
Inhomogeneous model	3.50–5.00	2.17–3.10	1.64–2.35
Other models	3.50	2.17	1.64
Source type	Double couple, $M_{xy} = M_{yx} = M_0$		
Source time function	Ricker wavelet		
Models	Gradient model	Inhom. model	Other models
Mean frequency	4.5 Hz	13.5 Hz	4.5 Hz
Source depth	12 500 m	2000 m	6000 m
FZ width	210 m	200 m	270 m
Grid spacing	30 m	10 m	30 m
Receiver spacing	100 m	20 m	100 m
Array aperture	2000 m	560 m	2000 m

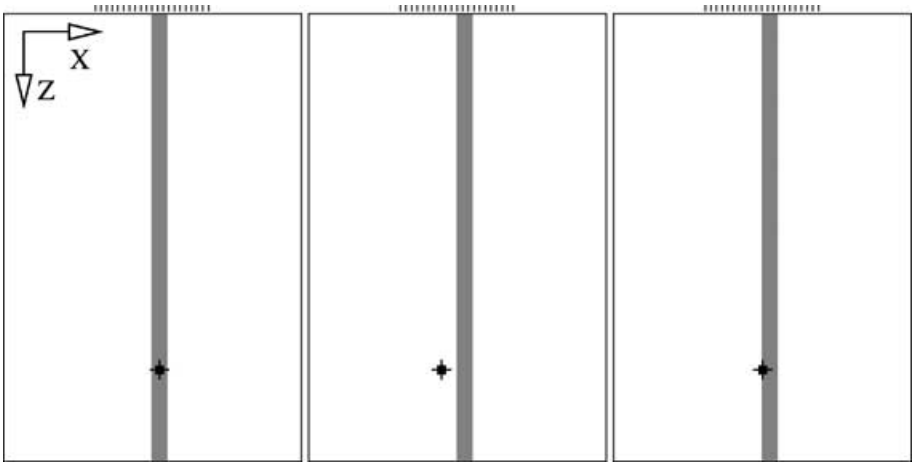

Figure 1. Model of a basic fault and different source locations. Left: source centred in the fault; middle: source outside the fault; right: source at the fault boundary. The source depth is 6 km. The width of the FZ is 270 m. The receivers are positioned along a line crossing the fault, marked by vertical dashes on top. The size of the model is 5 km in the x and y directions and 7.5 km in the z direction.

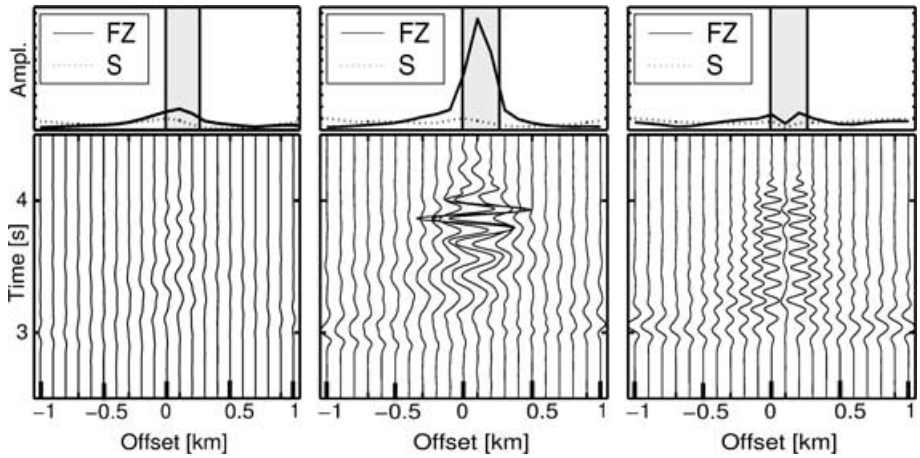

Figure 2. Seismograms for the models shown in Fig. 1. The y-component of velocity seismograms are drawn to scale. Left: source outside the fault, middle: source at the FZ boundary, right: source centred in the fault. The grey rectangle denotes the stations above the fault. The maximum amplitude of each trace for both the direct (dotted line, marked with an S) and the trapped wave (solid line, marked with FZ) are displayed on top of the seismograms.

most concentrated, the wave trains for the other models arrive more dispersed. The frequency spectrum for the source located outside the fault contains lower frequencies compared with the source at the FZ boundary, whereas the spectrum of the centred source is shifted to higher frequencies. A more extensive examination of the effect of source location with respect to a deep fault zone layer is given by Ben-Zion (1998). Unless stated otherwise, in the following 3-D simulations the source location will be at the FZ boundary.

3.2 Discontinuous faults

To answer the question of how continuous a fault must be to guide FZ waves, three models with different amounts of structural offset are examined (see Fig. 4). The model properties are described in Table 1. While the model setup is such that the waves travel vertically across the FZ discontinuity, this geometry may also be relevant for faults with a horizontal offset, a commonly observed feature at the surface. In the case of a lateral shift of half the FZ width, the amplitude distribution is similar to that of the basic fault model (Fig. 5) and a strong distinct peak in the amplitude distribution of the FZ waves appears. The spatial width of this peak is almost the same as in the basic fault model, but the amplitude is lowered from a 10-fold amplification for the basic model to an eightfold increase. For a shift of one FZ width, the maximum FZ wave amplitude increase is fourfold. In addition, the width of the region with higher amplitudes is broadened compared with the previous models to $\frac{3}{2}$ FZ widths. The model with a lateral shift of $\frac{3}{2}$ FZ widths shows only a 2.5-fold FZ wave amplitude increase, and the region with higher amplitudes extends over 2.5 FZ widths. The waveforms and traces in Fig. 6 show longer FZ wave trains with lower amplitudes for increasing fault offsets, indicative of increasing diffusion of the FZ waves for increasing structural discontinuity. The spectra of all models are similar.

3.3 Varying fault width

The next set of models are used to investigate the influence of varying FZ shape on the trapped waves. Fig. 7 shows three structures with a narrow part of variable size in the vertical direction, acting as a bottleneck for the propagating FZ waves. Additional model properties are described in Table 1. In all models the narrowest part is 40 per cent of the maximum FZ width, while the depth extension of the bottleneck varies from model A (largest extension) to model C (smallest extension). The maximum FZ width is 270 m.

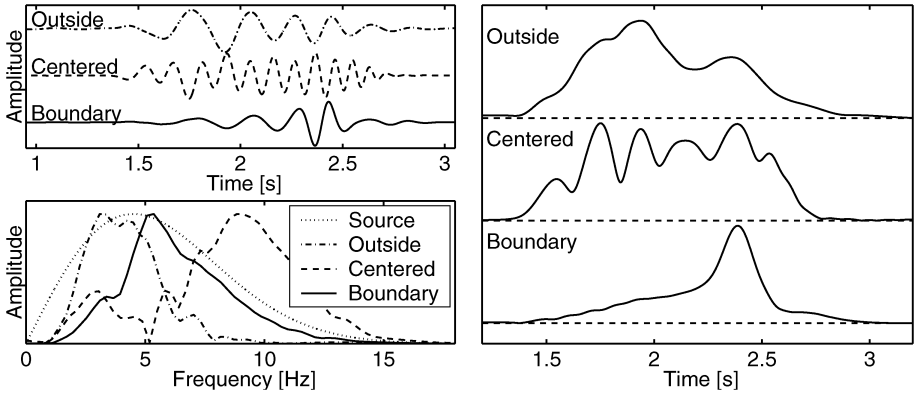

Figure 3. Left column: trace with the maximum FZ wave amplitude (top) and the corresponding amplitude spectrum for the models with different source locations (bottom). Solid: source at FZ boundary, dashed: source centred in the fault, dash-dotted: source outside. Dotted: spectrum of the source time function. Right column: corresponding envelopes of the traces. All graphs shown here are normalized. The relative amplitudes of the waves in the different cases are shown in Fig. 2.

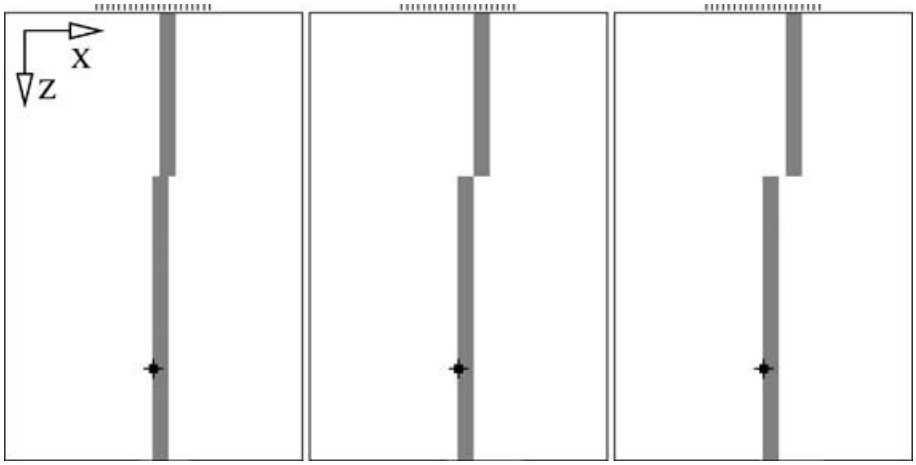

Figure 4. Fault models with different amounts of lateral disruption. Left: shift of $\frac{1}{2}$ FZ width, middle: shift of 1 FZ width, right: shift of $\frac{3}{2}$ FZ width. The size of the model corresponds to the models in Fig. 1.

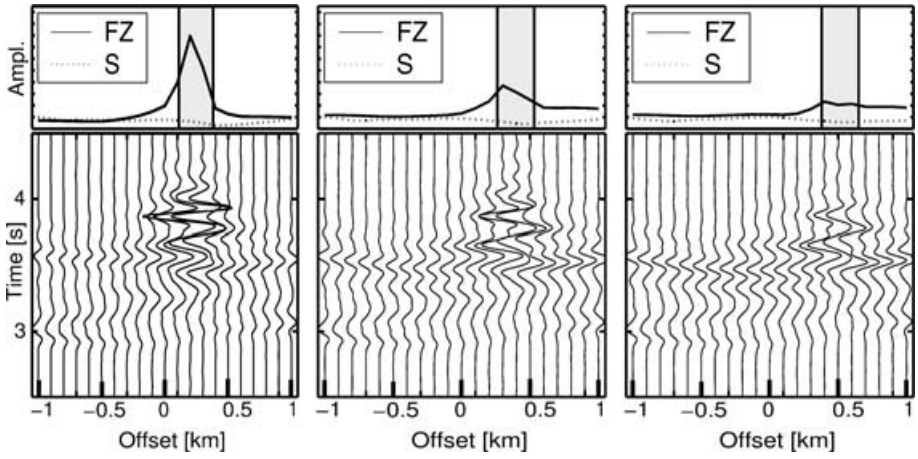

Figure 5. Seismograms and maximum amplitudes for the models shown in Fig. 4. Left: shift of $\frac{1}{2}$ FZ width, middle: shift of 1 FZ width, right: shift of $\frac{3}{2}$ FZ width.

In model A, with a large and narrow bottleneck extension of $13\frac{1}{3}$ FZ widths, the guided waves in the seismograms arrive slightly earlier than the FZ waves of the basic fault model (Fig. 8). For the first arrivals, this difference is only 0.1 s but the effect is somewhat larger for the strongest amplitude phases and the FZ waves for the bottleneck model arrive 0.2–0.25 s prior to the waves in the basic case. The maximum amplitude of the guided waves is fivefold and thus half as big as in the basic FZ case. For model B with

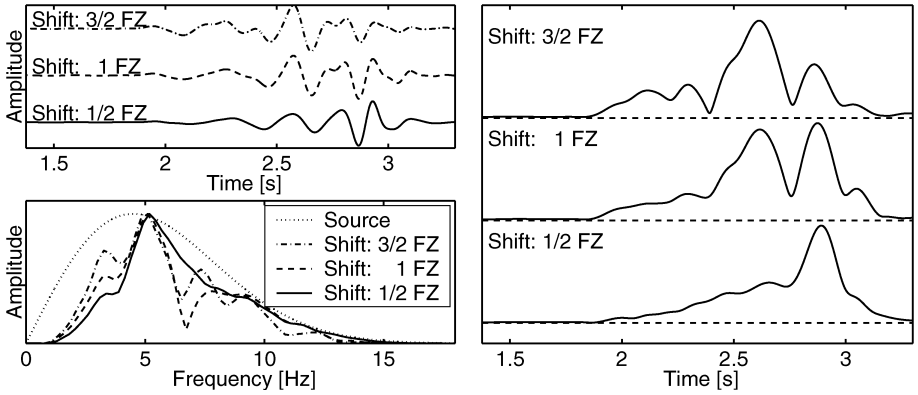

Figure 6. Seismograms, amplitude spectra and envelopes for the fault models with lateral disruption. Solid: shift of $\frac{1}{2}$ FZ width, dashed: shift of 1 FZ width, dash-dotted: shift of $\frac{3}{2}$ FZ width. Dotted: spectrum of the source time function.

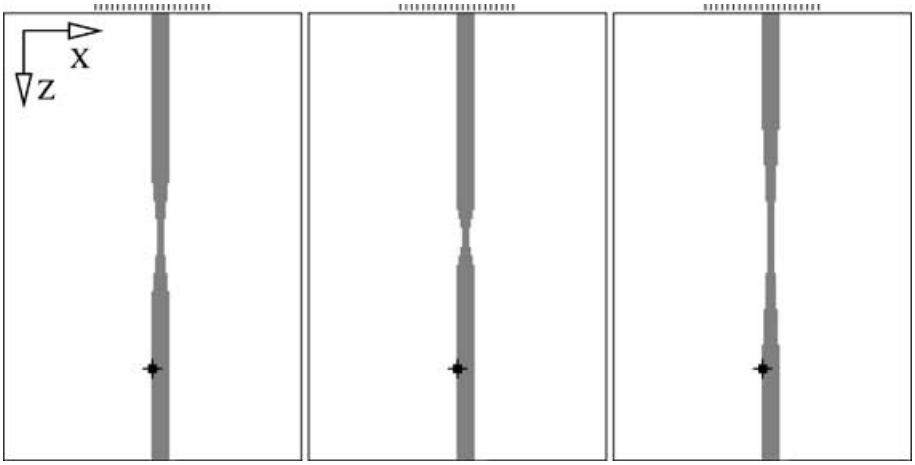

Figure 7. Models of a bottleneck with different extension in depth. Left: extension of $6\frac{2}{3}$ FZ widths; middle: extension of $3\frac{1}{3}$ FZ widths; right: extension of $13\frac{1}{3}$ FZ widths. The size of the model corresponds to the models in Fig. 1.

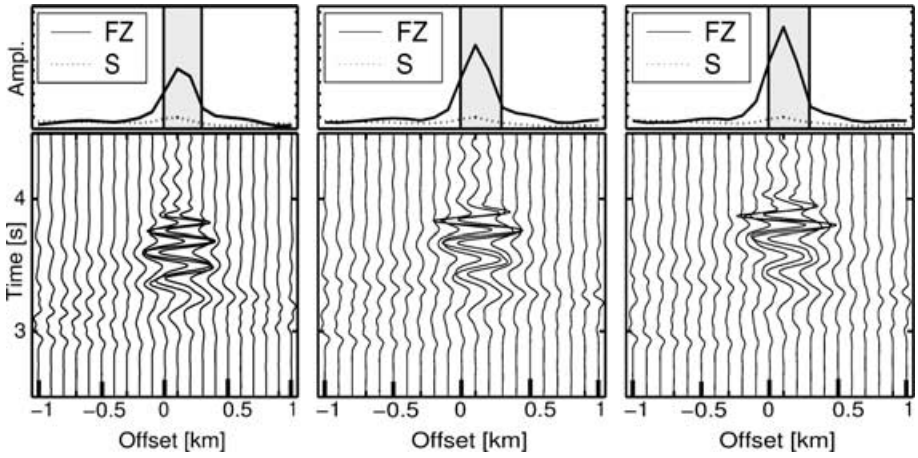

Figure 8. Seismograms for the models shown in Fig. 7. Left: extension of $13\frac{1}{3}$ FZ widths, middle: extension of $6\frac{2}{3}$ FZ widths, right: extension of $3\frac{1}{3}$ FZ widths.

a bottleneck extension of $6\frac{2}{3}$ FZ widths the trend of an earlier arriving FZ wave compared with the basic case still persists. Owing to the smaller extension of the narrow FZ part these effects are reduced to 0.1 s. The maximum FZ amplitude is seven times the *S*-wave amplitude. Model C with the smallest bottleneck extension of $3\frac{1}{3}$ FZ widths shows almost the same traveltimes and maximum FZ amplitudes as the basic fault model. The spectra of the three models show no significant difference, but the envelopes reveal an increasing length of the wave train for larger bottleneck extensions (Fig. 9).

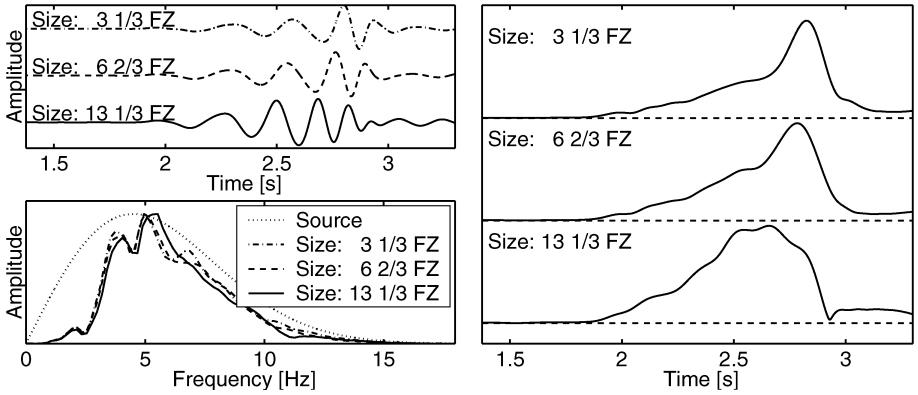

Figure 9. Seismograms, amplitude spectra and envelopes for the fault models with a bottleneck with a different extension in depth. Solid: extension of $13\frac{1}{3}$ FZ widths, dashed: $6\frac{2}{3}$ FZ widths, dash-dotted: $3\frac{1}{3}$ FZ widths. Dotted: spectrum of the source time function.

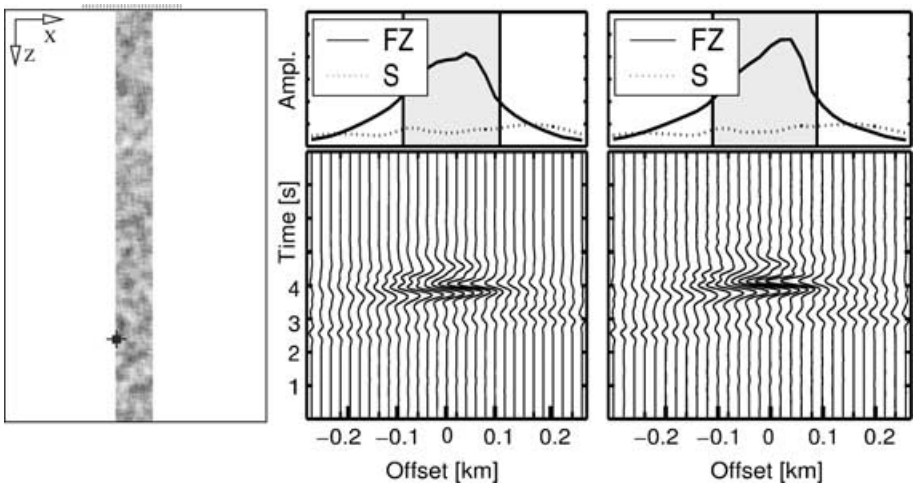

Figure 10. Left: model with small-scale inhomogeneities, the FZ properties vary from −30 to 0 per cent with respect to the surrounding quarter-spaces. Middle: seismograms for a reference model with uniform seismic FZ properties that corresponds to the average of the inhomogeneous model. Right: seismograms for a fault with small-scale inhomogeneities.

3.4 Small-scale inhomogeneities

In the models described so far, the material properties in the FZ were constant. In this section we investigate the influence of varying seismic properties at small scales in a simple FZ geometry. To be able to add small 3-D perturbations to a thin FZ layer, a denser grid with a spacing of 10 m and a FZ width of 200 m were chosen. Since the smaller grid spacing allows the computation of higher frequencies, the mean frequency source time function was set to 13.5 Hz. The model properties are described in Table 1. The inhomogeneous FZ region was produced by calculating a random number for each gridpoint belonging to the FZ and applying a spatial sliding window averaging $5 \times 5 \times 5$ neighbouring points. This process yields a heterogeneous model with a correlation length of ≈30 m. The smoothed random values were mapped to the desired velocity distribution in the fault. Fig. 10 (left) shows a cross-section through the FZ with a grey-scale proportional to the seismic velocity. The properties inside the FZ vary from −30 per cent (dark grey) to 0 per cent (white) with respect to the surrounding half-space. Fig. 10 (centre and right) shows seismograms of this model and of a corresponding FZ structure with seismic properties given by the average properties of the inhomogeneous model. The seismograms and distributions of FZ wave amplitude are similar in both cases. The FZ wave trains, spectra and traces envelopes (Fig. 11) also show no significant differences.

3.5 Low-velocity layer and vertical velocity gradient

FZs are expected to widen towards the surface owing to decreasing confining pressure and to be covered with a low-velocity layer caused by sedimentation. Models A and B (Fig. 12, left) explore this configuration. Earlier 2-D and symmetric 3-D modelling of similar structures can be found in Leary *et al.* (1991), Li & Vidale (1996) and Igel *et al.* (1997). The FZ width in the lower part of the model is 210 m and the source is located at 12.5 km depth. In both models, the same fault geometry is used and the velocities and the density of the fault is lowered by 25 per cent with respect to the background. Model A has uniform properties at depth, but in model B the velocities and the density increase with depth similarly to Fig. 6 of Ben-Zion *et al.* (1992) based on traveltime tomography for the Parkfield section of the San Andreas fault. At the bottom of model B the density and the velocities are 20 per cent higher than at the surface. A full description of model parameters is given in Table 1. In both models, the path-length of the trapped waves travelling through the fault is 60 FZ widths and thus is relatively long compared with the previous

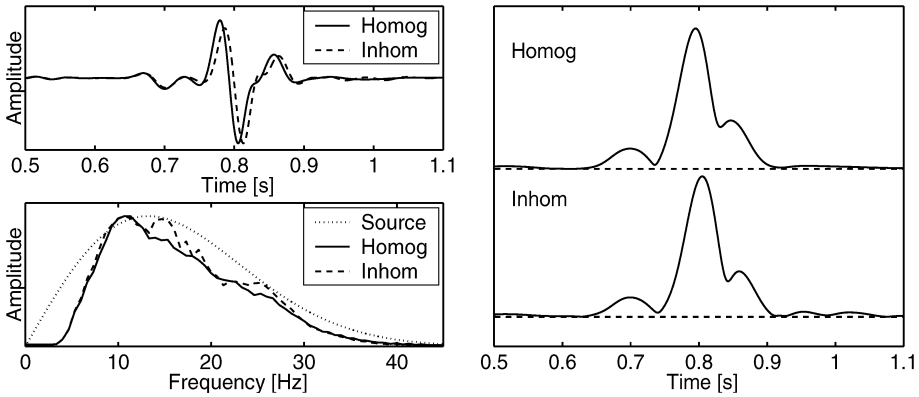

Figure 11. Seismograms, amplitude spectra and envelopes for the fault with small-scale inhomogeneities and a homogeneous reference model. Solid lines: reference model with the average seismic properties of the inhomogeneous model; dashed lines: model with small-scale inhomogeneities; dotted lines: spectrum of the source time function. Right-hand column: corresponding envelopes of the traces.

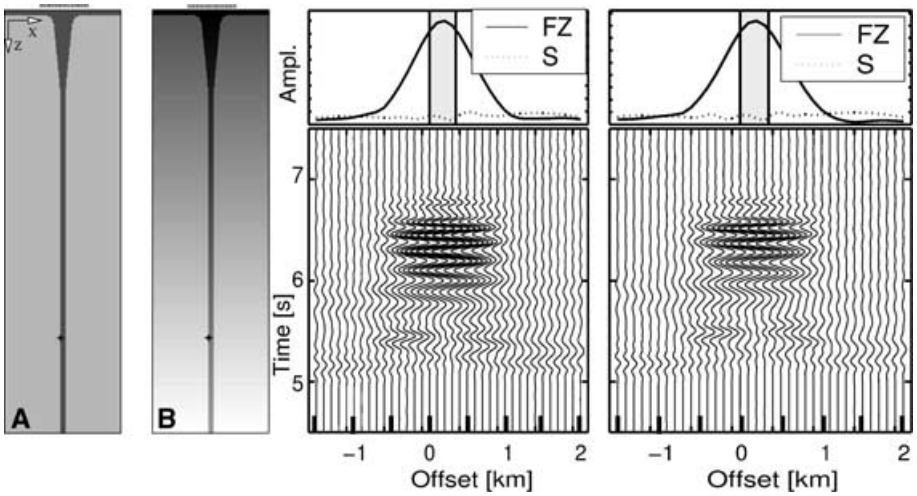

Figure 12. Left: models with a fault widening towards the surface and a low-velocity layer on top. The width at depth is 210 m and the width below the near-surface layer is 1170 m. The thickness of the low-velocity layer on top is 150 m. Model A: constant seismic properties with depth. Model B: velocities and density increase with depth. Middle: seismograms for Model A. Right: seismograms for model B.

models. In the absence of attenuation, the number of oscillations and hence overall duration of the FZ waves are proportional (for a fixed FZ width) to the length of the path inside the fault (Igel *et al.* 1997). High attenuation in the FZ, not accounted for here, will act as a low-pass filter, tending to reduce the complexity and duration of the FZ wave train with increasing path-length along the fault (Ben-Zion 1998). In Model A with uniform properties with depth the distribution of the amplitudes is approximately Gaussian with a half-length of three FZ widths (Fig. 12, centre). The size of the maximum FZ wave amplitude is eight times the *S*-wave amplitude. The seismograms in model B with increasing properties with depth are similar to those of the previous case (Fig. 12, right). The spectra and envelopes of traces show no significant differences with the only effect visible being a phase shift in the FZ waveforms (Fig. 13). Thus, fairly severe variations of material properties with depth are not significant variables for the generation and properties of FZ-guided waves.

3.6 The split-fault model

A common structural feature often visible at the surface is an offset separating two fault segments. However, the extent to which fault offsets seen at the free surface persist at depth is not generally known. Increasing confining pressure and temperature with depth may tend to lessen structural complexity such as fault offsets. Imaging the (dis)continuity of fault surfaces at depth is important for seismic hazard estimates because the largest possible event magnitude is likely to correlate with the extent of the continuous fault structure. Harris & Day (1993) and Li & Vidale (1996) examined, respectively, properties of dynamic rupture and FZ waves in models with surface structural offset that persist to depth. Here we analyse FZ-guided waves in a split-fault model (Figs 14 and 15) consisting of two segments that are offset at the surface but connected at depth. The depth of the bifurcation point of the segments is 3990 m and the source depth is 2010 m below the bifurcation point. Additional model properties are described in Table 1. The special case of a source centred underneath the two segments is discussed in Igel *et al.* (2002). The seismograms of the split-fault model are affected by: (1) different geometrical spreading caused by the array aperture and (2) the shape of the FZ. To be able to separate these two effects, a simulation of a basic fault with comparable source–receiver setup was performed (Igel *et al.* 2002). The main effect of the different distances from the source to each receiver line in the basic model are small changes to the arrival times. The effect of the receiver position

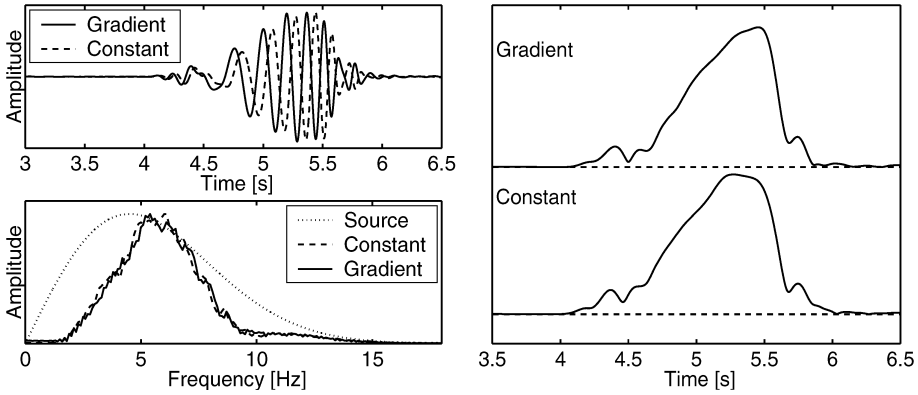

Figure 13. Left-hand column: trace with the maximum FZ wave amplitude (top) and the corresponding amplitude spectrum for a fault widening towards the surface and a low-velocity layer on top. Solid: model with increasing velocities and density with depth (gradient model), dashed: model with constant properties (constant model), dotted: spectrum of the source time function. Right-hand column: corresponding envelopes of the traces.

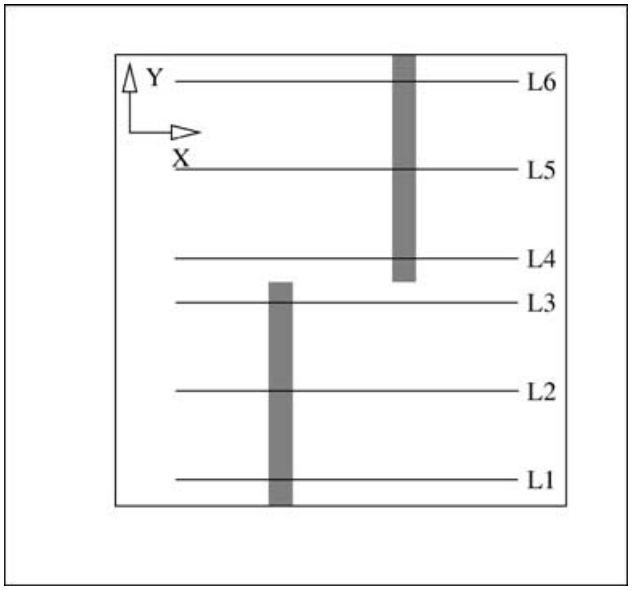

Figure 14. Map view of the locations of the receiver profiles and the discontinuity in the fault zone trace. Seismograms for these profiles are shown in Fig. 15.

along strike on the FZ amplitudes is negligible. In the simulations discussed below, the source location is shifted laterally 990 m along the fault in the *y*-direction away from the centre of the split. The source is located below one branch of the fault and trapped wave energy that is transmitted into the second branch has to pass below the bifurcation point. The location of the receiver profiles are given in Fig. 14 and the synthetic seismograms are shown in Fig. 15. The receivers at the branch on top of the source show a maximum FZ wave amplitude of four times the *S*-wave amplitude. FZ waves also arrive on top of the other branch with a maximum amplitude of 2.5 times the *S*-wave amplitude. Even with a source shifted towards one branch, trapped waves can be seen on top of both segments of the fault.

4 DISCUSSION

We now summarize and classify the results presented in the previous sections in terms of weak, moderate and strong effects of 3-D structural perturbations to a basic 2-D FZ. Then we discuss further results of the split-fault model and the implications of the parameter-space study of this work for imaging discontinuous FZ structures at depth.

4.1 Weak effects

In real fault structures one expects an increase of seismic velocities and density with depth. To analyse this, a linear gradient of seismic velocities and density was applied to models with a fault widening towards the surface and a horizontal low-velocity layer (Fig. 12 left, Model B). For both models the maximum FZ wave amplitude, the spectra and the trace envelopes resemble closely those of the basic FZ, the only difference being a phase shift of the FZ wavelets (Fig. 13). It thus seems that realistic vertical gradients of seismic properties have negligible effects on the FZ-guided waves.

The model with small-scale 3-D variations of the seismic properties within the FZ (Fig. 10, left) shows that FZ waves are almost unaffected by those perturbations. Despite the strong variation of the seismic properties inside the fault, clear FZ waves with considerable amplification develop. The FZ wave amplitudes, waveforms, spectra and envelopes are very similar to those in the homogeneous reference fault model with average seismic properties (Fig. 10, middle and right). Therefore, small-scale inhomogeneities with scalelengths considerably less than the dominant wavelength cannot be resolved from seismograms of guided waves. This result is in agreement with Igel *et al.* (1997) who suggested that trapped waves average out irregular FZ geometries with correlation lengths smaller than the FZ width.

4.2 Moderate effects

The influence of gradual variations of the FZ shape on the trapped waves is moderate. For shape perturbations that are not too strong, the resulting FZ wavefield is similar to that of an unperturbed fault. Since such modifications can be made in many ways, we focus on models with reduced FZ width at a certain depth (Fig. 7). The longer the guided waves travel in a FZ section with reduced width, the earlier these FZ waves arrive at the seismometer (Fig. 8). Also, the maximum FZ wave amplitude is reduced when the waves travel part of the way along a narrow FZ section, compared with the undisturbed FZ case. Given the large differences in the geometry of the considered models, the effect of gradual shape changes on the traveltime is negligible and the effect on the FZ wave amplitude is moderate. Overall, gradual variations of the FZ shape have less influence on guided waves than the source location and a lateral discontinuity of the fault.

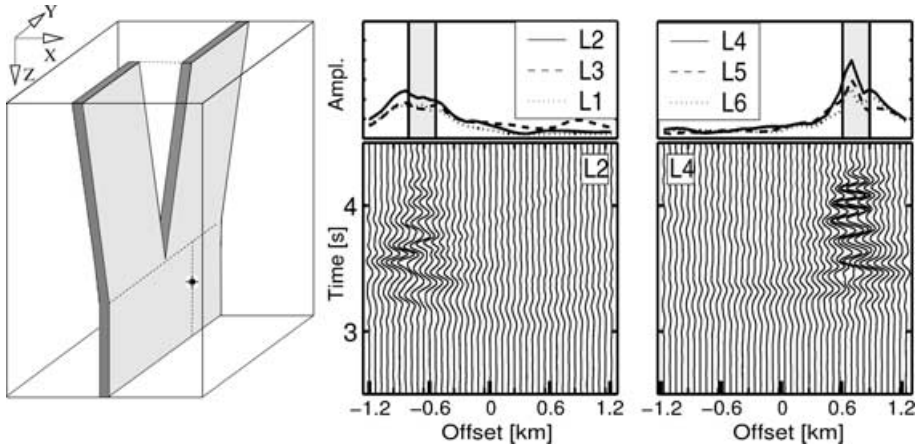

Figure 15. Left: split-fault model with the source shifted laterally. Middle: seismograms of receiver line L2 situated on top of the forepart of the fault. Right: seismograms for receiver line L4 situated on top of the rear part of the fault. The seismograms of the receiver line with the strongest FZ waves on each fault segment and the maximum amplitude distributions of all six receiver lines are shown. Even the stations on profile L1–3 of the fault show clear FZ wave arrivals.

The effect of a FZ widening towards the surface and merging with a horizontal low-velocity layer on top of the fault (Fig. 12 left, Model A) is also small to moderate. Such a FZ configuration leads to a Gaussian-shaped spatially smeared region of enlarged FZ wave amplitudes. This effect can also be seen in Leary *et al.* (1991), Li & Vidale (1996) and Igel *et al.* (1997). Because of the wider distribution of FZ wave energy, the maximum amplitudes are comparatively low. Without taking this subsurface structure into account one would image a broader fault zone with a lower velocity contrast by analysing FZ seismograms with 2-D models. In general, the 3-D ingredients discussed in Sections 4.1 and 4.2 produce minor and moderate forms of diffusion of the FZ waves, respectively.

4.3 Strong effects

The variation of source location with respect to a deep FZ can drastically influence the resulting wavefield. To quantify this, a basic fault with three different source locations was investigated (Fig. 1). The employed source mechanism corresponds to a localized strike-slip dislocation (double-couple). For this mechanism the strongest FZ amplitudes occur for sources located at the FZ boundary (Fig. 2). In contrast, a hypocentre location near the FZ centre leads to destructive interference of FZ waves and to small FZ wave amplitudes. Similar results were found by Ben-Zion (1998) using 2-D analytical calculations. If the source has an isotropic radiation pattern, no such destructive interference occurs and strong FZ wave amplitudes also develop for a source in the centre of the FZ (Li & Vidale 1996). Sources located outside the FZ with normal distances larger than the FZ width produce weak or no FZ waves. However, Ben-Zion (1998) showed that if the low-velocity FZ layer has an adjacent transition zone with intermediate properties between those of the FZ layer and the host rock, considerable trapped waves energy can be generated by sources in the transition zone that are far from the FZ core. In addition, Igel *et al.* (2002) and Fohrmann *et al.* (2001) also showed that sources below and well outside a shallow FZ layer can produce significant trapped waves in the shallow FZ layer, in contrast to earlier inferences (Li & Vidale 1996).

Another FZ parameter that influences strongly the resulting FZ waves is a lateral discontinuity of the fault (Fig. 4). For the model with a lateral offset of half a FZ width, the distribution of the FZ wave amplitudes mirrors the location and width of the upper part of the fault (Fig. 5). Analysing the seismograms without any knowledge of the underlying structure would lead to the correct fault width by assuming a simple, continuous fault. The slightly lower amplitudes of the FZ waves could lead to a slightly lower velocity contrast of the estimated simple fault structure. This loss of energy, which occurs at the fault disruption appears in the seismograms as arrivals spatially smeared out between *S* and FZ waves that can also be seen in the snapshots in Fig. 8 of Igel *et al.* (2002). For a lateral offset of 1 FZ width the FZ wave amplitudes are four times the *S*-wave amplitudes, that is 50 per cent of the amplitude of the previous model. The zone of increased amplitudes is less distinct compared with the previous model. For the model with a shift of $\frac{3}{2}$ FZ widths the amplitudes are less than 2.5 times the *S*-wave amplitudes. Therefore, in this case the amplitude is not a good indicator for distinguishing between trapped and direct *S* waves. Estimating the FZ width based on the zone with FZ waves would in this set-up lead to a threefold overestimation of FZ width and an underestimation of the velocity contrast by assuming a simple fault structure.

4.4 The split-fault model

The previous model is motivated by a central question concerning fault structures. Often two or more parallel fault segments that are separated by a gap perpendicular to the sections are visible at the surface and it is not clear whether these segments are connected at depth. The ability to image such structures would have important implications on the maximum expected earthquake size and a variety of other issues of earthquake and fault dynamics. If FZ waves generated by a given source are visible on different fault segments, these segments are likely to be connected at depth. Cases where this occurs are shown by Igel *et al.* (2002) for a source centred between the two segments, and in the present study for sources shifted from underneath the bifurcation point towards one fault segment. It is possible that for larger lateral shifts, trapped waves will be observed only on top of one segment. This will be examined in a future study.

4.5 Comparison with other studies

As the results presented contain new geometries, source–receiver setups and source types it is important to compare the conclusions and implications with those of previous studies.

Ben-Zion (1998) analysed the 2-D scalar wavefield for fault zones consisting of two vertical layers between two quarter spaces. The

source was an *SH* line dislocation oriented parallel to the fault structure. The study focused on clarifying effects of, and trade-offs between, propagation distance along the fault, FZ width, source position within the FZ, velocity contrast across the fault, attenuation coefficient of FZ material, receiver depth and normal offsets of source and receivers from the FZ. All of these variables were shown to have significant effects on FZ-guided waves, and thus all are important variables in inversions of observed guided waves. The analytical solution of Ben-Zion (1998) can be computed quickly and a large number of models can be tested in a systematic examination of the parameter space spanned by the above sensitive parameters. However, because of the restriction on the 2-D scalar wave equation, the method is limited to uniform fault structures and either *P*- or *SH*-wave propagation. Igel *et al.* (2002) demonstrated that another shortcoming of the 2-D analytical solution associated with the assumed line source can be corrected by applying a convolution filter. This was also shown by Li & Vidale (1996). Such a 2-D–3-D transformation filter may not work correctly for some complex structures and 3-D elastic waves (see Igel *et al.* 1993, for examples). Li & Vidale (1996) investigated 2-D fault models with an acoustic FD method for the *SH* wave equation. Their work focused on effects of structural discontinuities, surface layers and other heterogeneities in 2-D. Some of those models can be compared with the present study and show similar results, e.g. concerning the effect of the source radiation pattern, source location, surface layers, varying FZ width at depth and fault disruption. Igel *et al.* (1997) performed *SH*- and *P*–*SV*-wave propagation in cylindrical coordinates for axisymmetric models. The modelling focuses on the trade-off between the propagation distance of the FZ waves and the FZ width, the source location relative to the FZ, FZ widening towards the surface, a low-velocity surface layer, a horizontal velocity gradient within the FZ, a FZ with vertical heterogeneities and small-scale scatterers in the FZ. In the present work we extend the parameter-space study of Igel *et al.* (1997) to true 3-D cases and examine the effects of source location with respect to the fault, FZ width, FZ velocity contrast, varying the FZ width with depth, a FZ capped at the surface, discontinuous faults and shallow fault structures. The following statements summarize our results and those of Igel *et al.* (1997, 2002):

(1) FZ waves are highly sensitive to the source location with respect to a FZ continuous with depth;

(2) a low-velocity surface layer can distort and attenuate FZ waves;

(3) gradual variations of the FZ properties such as velocity gradient and shape have minor influences on the trapped waves;

(4) a lateral disruption of more than one FZ width can reduce the efficiency of FZ wave propagation considerably;

(5) a shallow FZ is capable of trapping significant seismic energy from deeper sources in the surrounding medium;

(6) varying the source location within the FZ has a strong effect on the radiation pattern and thus the efficiency for generating trapped waves;

(7) faults with increasing width towards the surface showed a spatial smearing and a decrease in amplitude; and

(8) small-scale scatterers do not obstruct the trapping efficiency of faults.

5 CONCLUSIONS

Currently, the structure of fault zones at depth is not well understood. Seismic FZ waves may be one of the best diagnostic tools for imaging fault structures. Observed FZ-guided waves can be well explained and interpreted using simplified 2-D FZ structures (e.g. Hough *et al.* 1994; Li *et al.* 1994; Michael & Ben-Zion 1998; Peng *et al.* 2000). This is perhaps not surprising since an ideal seismic waveguide is 2-D and thus FZ waves will not exist in structures that are too heterogeneous to be approximated in 2-D over a given spatial extent and for the relevant frequencies. To clarify how various realistic deviations from the 2-D cases would alter the wavefield, we have analysed a set of FZ models starting from a basic FZ and varying different geometrical and seismic properties separately to understand the influence of these variations on the FZ wavefield. Some of these variations were combined in a study of a structure consisting of a fault that splits into two fault segments towards the surface. In agreement with previous studies based on 2-D analytical and numerical calculations (Ben-Zion 1998; Li & Vidale 1996), we find that a source location inside a fault does not necessarily lead to strong FZ wave amplitudes. Depending on the location with respect to the FZ boundaries, the radiated wavefield may interfere destructively, leading to low FZ wave amplitudes. Some additional effects previously investigated with 2-D and symmetric 3-D methods (e.g. Leary *et al.* 1991; Li & Vidale 1996; Igel *et al.* 1997) can be confirmed: FZ waves are highly sensitive to the source location with respect to a FZ continuous with depth. A shift of the source location by less than the wavelength may lead to strong variations of the FZ waves. Yet, from this we may not conclude that FZ-guided waves cannot be generated by sources outside the core of the FZ. As shown by Ben-Zion (1998), sources in a transition zone bounding a FZ layer can produce considerable trapped-waves energy. In addition, dislocation sources located outside and below a shallow vertical low-velocity layer by many FZ widths can lead to trapping of considerable seismic energy in the shallow structure (Fohrmann *et al.* 2001; Igel *et al.* 2002). These results have important implications and they differ from earlier inferences made by Li & Vidale (1996).

Moderate effects occur for variations of the internal shape of the fault. No significant influence on the FZ wave propagation is caused by small-scale inhomogeneities inside the fault or a realistic vertical velocity gradient. A 3-D fault zone that is continuous with depth and forks into two segments towards the surface is capable of guiding FZ waves in both segments as long as the source is below the bifurcation. Otherwise, if the fault has a disruption greater than the FZ width, trapped energy is not able to propagate efficiently across this gap and no large amplitudes caused by FZ waves occur. Thus the simultaneous detection of FZ waves on different fault segments indicates that these segments are connected at depth. This information is important for estimating the overall size of a connected FZ and thus the maximum magnitude of an earthquake occurring on that fault.

Calculations of elastic 3-D wave propagation in fault zones provide an important tool for understanding the properties of seismic waves in irregular FZ structures, the design of new field experiments and for modelling observed data. Our results indicate that detailed 3-D variations of fault zone structure of the type inferred (e.g. Li *et al.* 2000; Li & Vernon 2001) from analysis of trapped waves can probably not be resolved by the guided-waves data employed. This is especially so given the strong trade-offs between average 2-D model parameters (Ben-Zion 1998; Michael & Ben-Zion 1998) and additional observational uncertainties (e.g. the source mechanism and location). The depth extent of fault zone structures generating the observed trapped waves is also unresolved at present. We note that recent analyses of trapped waves in the Karadere-Duzce branch of the North-Anatolian fault, the Parkfield segment of the San Andreas Fault and the rupture zone of the 1992 Landers earthquake

(Ben-Zion *et al.* 2002, and references therein) indicate that the generating structures are shallow and or isolated low-velocity regions rather than deep coherent layers that span the seismogenic zone. Detailed knowledge of FZ structure at depth is important for shaking hazard assessments, the estimation of likely earthquake magnitudes and the dynamic behaviour of future large earthquakes. Progress in obtaining such knowledge will require careful additional observational and theoretical studies.

6 SUPPLEMENTARY MATERIAL

Supplementary material is available from http://www.blackwell-science.com/products/journals/suppmat/GJI/GJI1784/index.html

ACKNOWLEDGMENTS

We gratefully acknowledge the Enigma Project for High Performance Computing in Geophysics at the Institute of Theoretical Geophysics in Cambridge and the Leibniz Rechenzentrum in Munich for access to their supercomputers. YBZ acknowledges support from the Southern California Earthquake Center (based on NSF cooperative agreement EAR-8920136 and USGS cooperative agreement 14-08-0001-A0899). We thank John Vidale, Christian Haberland and Michael Korn for constructive comments. We also acknowledge the German Academic Exchange Service for supporting YBZ through the International Quality Network: Georisk.

REFERENCES

Ben-Zion, Y., 1989. The response of two joined quarter spaces to, *SH* line sources located at the material discontinuity interface, *Geophys. J. Int.,* **98,** 213–222.

Ben-Zion, Y., 1990. The response of two half spaces to point dislocations at the material interface, *Geophys. J. Int.,* **101,** 507–528.

Ben-Zion, Y., 1998. Properties of seismic fault zone waves and their utility for imaging low-velocity structures, *J. geophys. Res.,* **103,** 12 567–12 585.

Ben-Zion, Y., 1999. Corrigendum: the response of two half spaces to point dislocations at the material interface by Ben-Zion (1990), *Geophys. J. Int.,* **137,** 580–582.

Ben-Zion, Y. & Aki, K., 1990. Seismic radiation from an, *SH* line source in a laterally heterogeneous planar fault zone, *Bull. seism. Soc. Am.,* **80,** 971–994.

Ben-Zion, Y. & Malin, P., 1991. San Andreas fault zone head waves near Parkfield, California, *Science,* **251,** 1592–1594.

Ben-Zion, Y. & Sammis, C.G., 2002. Characterization of fault zones, *Pure appl. Geophys.,* in press.

Ben-Zion, Y., Katz, S. & Leary, P.C., 1992. Joint inversion of fault zone head waves and direct, *P* arrivals for crustal structure near major faults, *J. geophys. Res.,* **97,** 1943–1951.

Ben-Zion, Y., Peng, Z., Okaya, D., Seeber, L., Armbruster, J.G., Ozer, N., Michael, A.J., Baris, S. & Aktar, M., 2002. A shallow fault zone structure illuminated by trapped waves in the Karadere-Duzce branch of the North Anatolian Fault, western Turkey, *Geophys. J. Int.,* submitted.

Cormier, V.F. & Beroza, G.C., 1987. Calculation of strong ground motion due to an extended earthquake source in a laterally varying structure, *Bull. seism. Soc. Am.,* **77,** 1–13.

Cormier, V.F. & Spudich, P., 1984. Amplification of ground motion and waveform complexities in fault zones: examples from the San Andreas and Calaveras faults, *Geophys. J. R. astr. Soc.,* **79,** 135–152.

Fohrmann, M., Jahnke, G., Igel, H. & Ben-Zion, Y., 2001. Guided waves generated by sources outside a low velocity fault zone layer, *EOS, Trans. Am. geophys. Un.,* **82**, F886.

Fukao, Y., Hori, S. & Ukawa, M., 1983. A seismological constraint on the depth of basalt–eclogite transition in a subducting oceanic crust, *Nature,* **303,** 413–415.

Harris, R.A. & Day, S.M., 1993. Dynamics of fault interaction: parallel strike-slip faults, *J. geophys. Res.,* **98,** 4461–4472.

Hough, S.E., Ben-Zion, Y. & Leary, P.C., 1994. Fault-zone waves observed at the Southern Joshua Tree earthquake rupture zone, *Bull. seism. Soc. Am.,* **8,** 761–767.

Huang, B.S., Teng, T.-L. & Yeh, Y.T., 1995. Numerical modeling of fault-zone trapped waves: acoustic case, *Bull. seism. Soc. Am.,* **85,** 1711–1717.

Igel, H., Mora, P., Rodriguez, D. & Leary, P.C., 1991. Finite-difference simulation of fault zone trapped waves on the massively parallel Connection Machine (abstract), *EOS, Trans. Am. geophys. Un.,* **72**, 307.

Igel, H., Debski, W., Djikpesse, H. & Tarantola, A., 1993. Gradient inversion of marine seismic reflection data: parameterization and geometrical spreading, *Society of Exploration Geophysicists, Meeting 1993, Technical Programme,* 657–660.

Igel, H., Ben-Zion, Y. & Leary, P., 1997. Simulation of *SH*- and *P–SV*-wave propagation in fault zones, *Geophys. J. Int.,* **128,** 533–546.

Igel, H., Jahnke, G. & Ben-Zion, Y., 2002. Numerical simulation of fault zone trapped waves: accuracy and 3-D effects, *Pure appl. Geophys.,* **159,** 2067–2083

Leary, P.C., Li, Y.-G. & Aki, K., 1987. Observations and modeling of fault zone fracture anisotropy, *I*, *P SV, SH travel times*, *Geophys. J. R. astr. Soc.,* **91,** 461–484.

Leary, P.C., Igel, H. & Ben-Zion, Y., 1991. Observation and modeling of fault zone trapped waves in aid of precise precursory microearthquake location and evaluation, *Earthquake Prediction: State of the Art, Proceedings International Conference, Strasbourg, France,* 15–18 October 1991, pp. 321–328.

Leary, P.C., Igel, H., Mora, P. & Rodrigues, D., 1993. Finite-difference simulation of trapped wave propagation in fracture low-velocity layers, *Can. J. Expl. Geop.,* **29,** 31–40.

Li, Y.-G. & Leary, P.C., 1990. Fault zone seismic trapped waves, *Bull. seism. Soc. Am.,* **80,** 1245–1271.

Li, Y.G. & Vernon, F.L., 2001. Characterization of the San Jacinto fault zone near Anza, California, by fault zone trapped waves, *J. geophys. Res.,* **106,** 30 671–30 688.

Li, Y.-G. & Vidale, J.E., 1996. Low-velocity fault-zone guided waves: numerical investigations of trapping efficiency, *Bull. seism. Soc. Am.,* **86,** 371–378.

Li, Y.-G., Vidale, J.E., Aki, K., Marone, C.J. & Lee, W.H.K., 1994. Fine structure of the Landers fault zone: segmentation and the rupture process, *Science,* **265,** 367–370.

Li, Y.-G., Vidale, J.E., Aki, K., Xu, F. & Burdette, T., 1998. Evidence of shallow fault zone strengthening after the 1992 M7.5 Landers, California earthquake, *Science,* **279,** 217–219.

Li, Y.G., Vidale, J.E., Aki, K. & Xu, F., 2000. Depth-dependent structure of the Landers fault zone from trapped waves generated by aftershocks, *J. geophys. Res.,* **105,** 6237–6254.

Michael, A.J. & Ben-Zion, Y., 1998. Inverting fault zone trapped waves with a genetic algorithm, *EOS, Trans. Am. geophys. Un.,* **79**, F584.

Peng, Z., Ben-Zion, Y. & Michael, A.J., 2000. Inversion of seismic fault zone waves in the rupture zone of the 1992 Landers earthquake for high resolution velocity structure at depth, *EOS, Trans. Am. geophys. Un.,* **81**, F1146.

Virieux, J., 1984. *SH*-wave propagation in heterogeneous media: velocity-stress finite-difference method, *Geophysics,* **49,** 1933–1957.

Virieux, J., 1986. *P– SV* wave propagation in heterogeneous media: velocity-stress finite-difference method, *Geophysics,* **51,** 889–901.